Growth of Ultralong ZnS/SiO_2 Core−Shell Nanowires by Volume and Surface Diffusion VLS Process

Daniel Moore, Jenny Ruth Morber, Robert L. Snyder, and Zhong Lin Wang*

School of Materials Science and Engineering, Georgia Institute of Technology, Atlanta, Georgia 30332-0245

Received: October 10, 2007; In Final Form: December 3, 2007

Nanowires of up to 1 cm in length and approximately 30 nm in diameter were synthesized through a simple chemical vapor deposition process. Scanning electron microscopy (SEM) data showed that these nanowires were well-aligned and grew in the direction along the flow of the carrier gas. Through transmission electron microscopy (TEM) and X-ray diffraction (XRD) analysis, the nanowires were found to be composed of a single-crystalline ZnS core and amorphous SiO_2 shell. Gold catalyst particles were found at the tips of the nanowires and completely encased by a silica shell. Photoluminescence (PL) measurements were performed on nanowire samples in which the synthesis time was systematically varied to provide information regarding growth dynamics. After a systematic study on the structure, we propose that the core−shell nanowires were formed via a distinct volume and surface diffusion process occurring simultaneously for different chemical species in and on the gold catalyst particle.

Introduction

One-dimensional nanostructures such as nanowires and nanobelts have been suggested as ideal candidates for many electrical and optical applications, and several groups have reported successful synthesis in recent years.[1−13] In particular, semiconducting and II−VI nanowires have drawn large interest because of the ability to synthesize them in diverse configurations and under varying conditions, in addition to their potential use in numerous electronic and optical devices.[1,2,6] Zinc sulfide (ZnS), a member of the wurtzite family, is a direct wide band gap (3.91 eV) II−VI semiconductor and a vital material in the field of photonics. ZnS is also an important phosphor host lattice material used in electroluminescent devices (ELD), due to its large band gap, which enables emission of visible light without absorption and efficient electron transport. Furthermore, single ZnS nanobelts have been shown to facilitate optically pumped lasing.[2] The successful application of ZnS quantum dots in several biological studies indicates that nanowires and nanobelts of this material may also find practical use in areas such as biosensors, multiple cell or protein tagging, and even in vivo imaging and therapeutics.[14−19]

Still, the extensive reports of one-dimensional nanostructure growth have revealed several challenges that remain before these tools may practically be applied to commercial or industrial needs. One of these challenges arises from difficulty in producing very long nanowires that can be easily integrated and manipulated postsynthesis through simple methods. Another challenge is the need to organize such long nanostructures in ordered or aligned patterns and in high densities, further augmenting ease of use and scale-up.[1] Meeting both of these obstacles would significantly advance the development of one-dimensional nanostructures toward commercial and industrial utilization.

In addition, since the discovery of 1D nanostructures grown via catalyst-assisted physical vapor deposition (PVD) processes, researchers have been troubled to identify precise formation mechanisms, especially regarding the role of the metal catalyst particle. In a much earlier work, Wagner and Ellis outlined for the Au−Si system what is generally regarded today as the classic vapor−liquid−solid (VLS) nanowire growth mechanism, in which a diffusing species is transmitted through the bulk of a metal catalyst in liquid phase before incorporating into the growing nanowire.[20] Such a process may be easily applied to other dual component systems,[21] which often,[22,23] but not always,[24] appear to mimic the Au−Si model system. Growth mechanisms in multiple component systems, however, have proved much more difficult to conclusively identify, as in many cases the final product is not well-explained by this VLS process. In addition, these complex systems often lack experimental phase diagrams necessary to determine solubilities of diffusing species in the catalyst material, preventing easy identification of the conditions necessary for true VLS growth.

Several alternative mechanisms have been proposed for catalyst-assisted nanowire growth, often varying according to experimental parameters and growth species. The most applicable for our system, those in which ZnS or SiO_2 1D nanostructures grow via Au catalysis, vary across the literature and include several atomic transport schemes.[6,9−11,25−27] Such variance reveals a lack of consensus regarding the phase condition of the metal catalyst particle at elevated temperature, the diffusion mechanism in the metal catalyst, the role of transverse growth, and the state of the arriving gas species, among other issues. One source of discrepancy may be that growth mechanisms may vary according to the growth chemistry and parameters and may utilize not just one but a combination of processes. We examine previous investigations into the growth of 1D ZnS and SiO_2 nanowires and compare these findings to our own experimental evidence to arrive at a dual-diffusion mechanism for our core−shell nanowire samples.

In this paper, we report a large scale synthesis of laterally aligned, ultralong crystalline ZnS nanowires covered by an amorphous silica (SiO_2) shell. This work represents a novel synthesis of such nanowires exhibiting both dense and well-

* Corresponding author. E-mail: zhong.wang@mse.gatech.edu.

10.1021/jp709903b CCC: $40.75
Published on Web 02/05/2008

aligned organization while maintaining high aspect ratios. These nanowires, with lengths on the order of 1 mm to 1 cm, are long enough for simple manipulation into devices, addressing an essential need. The single-crystalline nature of the ZnS core ensures high-quality semiconductor material characteristics, while the amorphous silica shell should help to prevent mechanical or radiation damage and suppress chemical reactivity, which often leads to oxidation and contamination in bare ZnS nanomaterials. For biorelated applications, the low toxicity of both ZnS and silica is highly desired. In fact, some researchers have found that amorphous SiO_2 demonstrates low toxicity even in systems that do not respond well to its crystalline form.[28]

A series of systematic experiments coupled with careful analysis, including transmission electron microscopy (TEM), X-ray diffraction (XRD), and photoluminescence (PL), allow us to examine how variations in synthesis time affect the nanowire growth. These experimental measurements are used to help formulate a proposed growth mechanism. We propose a novel dual-diffusion process in which ZnS atoms migrate to the growing nanowire core via bulk diffusion through the gold catalyst particle, while the SiO_2 species migrate around the particle surface before becoming incorporated into the amorphous nanowire shell. Although initially several other routes leading to the growth of such core−shell nanowires could be envisioned, we eliminate each of these through careful examination of the final growth product. Finally, we test the theoretical feasibility of this model through diffusion calculations and find that the results support our proposed process.

Experimental Procedures

Synthesis of the ZnS/SiO_2 nanowires was carried out via a simple vapor deposition process. Commercially available ZnS powder (Alfa Aesar, 99.99% purity, metal basis) was placed in the center of a single-zone horizontal tube furnace (Thermolyne 79300), where the atmosphere, evaporation time, pressure, and temperature were controlled. Single-crystal silicon substrates with 20 nm of gold deposited by thermal evaporation were placed "downstream" at a lower temperature region in the furnace. Using a rotary vacuum pump, a vacuum was pulled in the tube for several hours to purge oxygen from the chamber. After evacuation to a pressure of about 2×10^{-3} Torr, the temperature in the center of the tube was elevated to 1000 °C at a rate of 50 °C/min. A N_2 gas flow was introduced into the system at a rate of 50 standard cm^3/min (sccm). The pressure in the system was allowed to increase to a value of 20 Torr and was held at that level through the duration of the synthesis. The silicon substrates reached a temperature of about 750 °C, as determined through prior thermocouple studies. After these conditions were maintained for between 1 and 2 h, the N_2 gas flow was turned off and a vacuum with a pressure around 2×10^{-3} Torr was again achieved. At this time, the furnace was allowed to cool to room temperature.

Optically, each sample appeared as a thick deposition of white powder or fluffy white fibrous material covering the silicon substrate. Samples growing for longer times showed increased deposition density on the substrates, with some deposition masking the silicon wafer completely. Some samples exhibited deposition product several millimeters past the silicon substrate. Care was taken when preparing samples for analysis not to destroy or contaminate the as-grown nanowires. Samples were analyzed initially using XRD and scanning electron microscopy (SEM). Initial XRD scans were fast scans (~10 min/sample) performed to determine basic phase information. Longer subsequent scans were then taken to gather more in-depth information from the samples. The SEM used for our analysis was a LEO 1530, operated at 5 kV. The samples were also examined using TEM (Hitachi HF-2000 operated at 200 kV).

X-ray diffraction measurements were performed on each sample using a PANalytical X-Pert Pro MRD X-ray machine with Cu Kα radiation. As-grown samples previously affixed to aluminum SEM stubs with carbon tape were loaded into the sample holder for solid samples affixed to the MRD cradle. Alignment was then performed via manual scans to check the sample position with respect to the 2θ, Z, and ω axes. Sample offsets were input into the system to calibrate zero positions for each axis. In this way, the sample was aligned parallel to the beam without the necessity to perform otherwise potentially destructive sample preparation.

For the measurements, the radiation beam emitted from an X-ray tube set to line focus, coupled with a parabolic mirror and 1/8° fixed divergence slits, was directed toward the unmodified nanowire coated substrate. After interaction with the sample, a 0.27 deg parallel plate collimator with a flat graphite crystal diffracted beam monochromator helped refine the signal before reaching the Miniprop large window point detector. The $2\theta-\omega$ measurements were taken with a tube power of 45 kV and 40 mA, from 5 to 120° in 2θ with a 0.01° step size and a 2 h and 23 min total scan time.

Results

SEM images like those illustrated in Figures 1 and 3 identified the synthesis product as nanowires aligned laterally to the substrate and in the direction of the N_2 gas flow in the tube furnace. Additionally, these images show that the aligned nanowires on the top layer of the substrate are fine and very long. Figure 1a−d reveals several images of a single representative nanowire sample. Figure 1a shows a composite SEM image taken across the ~1 cm deposition substrate. As shown in this figure, the nanowires are aligned along the flowing direction of the carrier gas. It appears that some nanowires begin at the leading edge of the substrate and continue well past substrate edge, making these nanowires approximately 1.5 cm in length. It was attempted to follow an individual nanowire by microscopy along the entire length of the substrate; however, in every attempt, the nanowire was lost about two-thirds of the way due to SEM image shift. Figure 1b contains an optical image of this sample, illustrating the length and density of the nanowires at low magnification. Note that the silicon substrate is completely masked by the nanowire sample. Figure 1c illustrates an SEM image of the substrate's leading edge. Figure 1b,d confirms that the nanowires grew beyond the substrate. Note that the boundary observed in Figure 1d corresponds to the edge of the sample stub, seen at the far right of Figure 1b, rather than the edge of the silicon substrate. The EDS profile taken in the SEM, seen in the inset, reveals the presence of Zn, S, Si, and O in the sample.

TEM images and electron diffraction patterns are presented in Figure 2. Several nanowires were imaged using low-resolution TEM, as shown in Figure 2a−c. The images shown in Figure 2a,b show the tip of the nanowire, including the terminating metal catalyst particle. EDS scans across the area of the particle (not shown) indicated the presence of Zn, S, Si, O, and Au. Note the contrast change seen in the amorphous shell layer at the tips of these nanowires. This contrast change in the 2D TEM projection seems to indicate the presence of a sphere or half-sphere of amorphous material surrounding the metal particle. The "neck" region of the nanowire just below the particle in Figure 2a is also of interest. Figure 2c shows a slightly higher

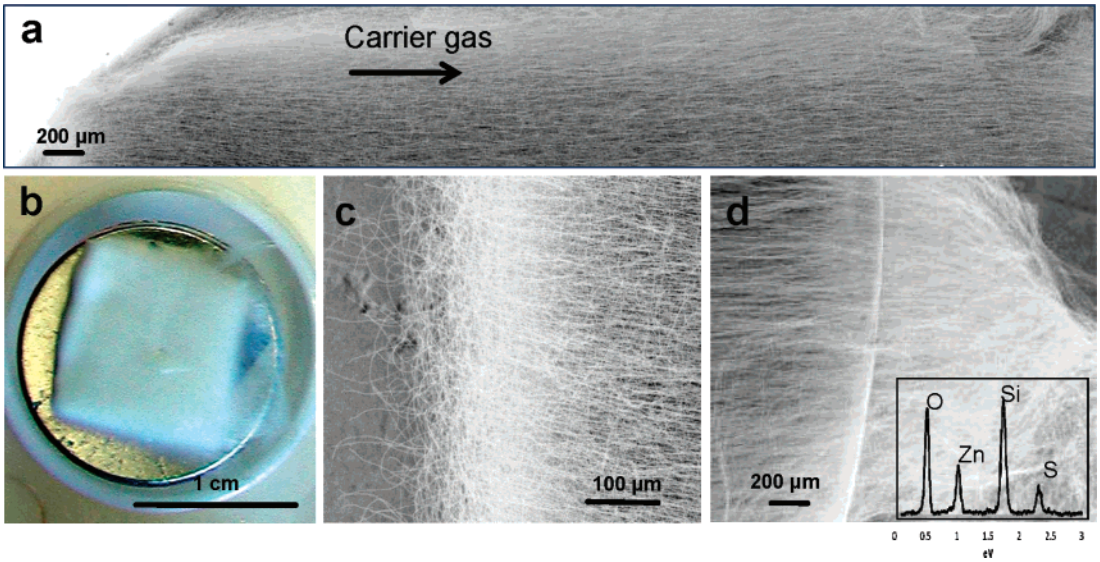

Figure 1. SEM and optical images showing a representative sample of ultralong ZnS−SiO_2 nanowires: (a) composite of several SEM images demonstrating nanowires length; (b) optical image taken from above sample, fixed on metal stub; (c) SEM image of the sample's leading edge; (d) SEM image of opposite edge, showing long nanowires reaching past the metal stub. The inset shows corresponding EDS data.

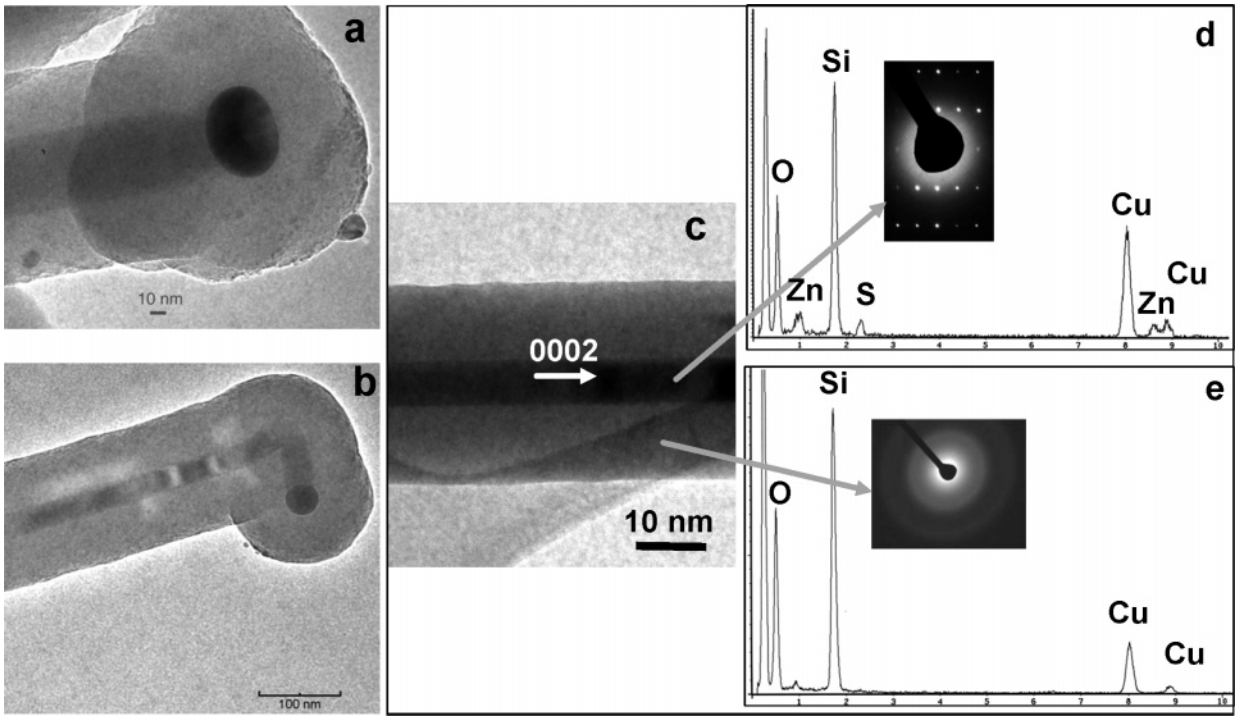

Figure 2. (a, b) Low-magnification TEM images showing the tip of two ZnS− SiO_2 core−shell nanowires, including the terminating metal particle. (c) Low-magnification TEM image of a nanowire center. (d) Electron diffraction pattern and corresponding EDS data from the nanowire illustrating the single-crystalline nature of the core. (e) Electron diffraction pattern and corresponding EDS data from the nanowire shell, showing the shell to be amorphous in nature and consisting of only Si and O.

magnification image of a nanowire center. Electron diffraction patterns were taken of the core and shell areas of this nanowire and are presented in Figure 2d,e, respectively. The electron diffraction pattern shown in Figure 2d, together with the EDS data also taken in the TEM, reveals that the nanowire core consists of a wurtzite-structured ZnS. The presence of Cu seen in the EDS spectrum is likely due to the Cu TEM grid used to affix the sample. Using analysis of the electron diffraction pattern, it was also determined that the ZnS core of the nanowire grew along the [0001] direction, the fast growth direction of wurtzite ZnS. Figure 2e shows TEM and EDS information corresponding to the shell of the nanowire sample. The electron diffraction pattern indicates that the shell is made up of an amorphous material, while the EDS graph shows presence of Si and O but not Zn or S. These results indicate that the nanowire is composed of a crystalline ZnS core and an amorphous SiO_2 shell.

To gain insight regarding the growth mechanism of these core−shell nanowires, synthesis at different time periods was conducted in an effort to observe the growth evolution of the nanowire structures. Synthesis runs were performed in which the maximum reaction chamber temperature was maintained for 15, 30, 45, 60, 90, and 110 min. To ensure that results were consistent and reproducible, at least three experiments were run for each set of parameters. The uniformity of the results observed in these experiments suggests a high degree of repeatability in

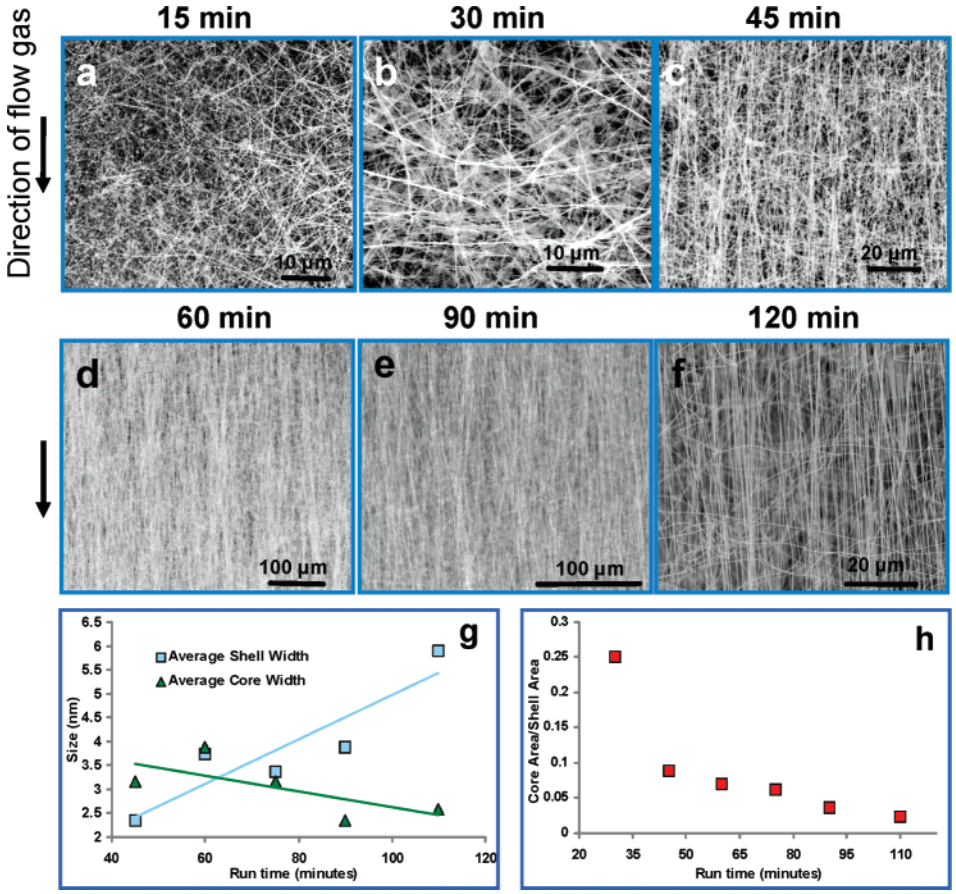

Figure 3. Ultralong nanowires as a function of growth time. SEM images show sample characteristics after (a) 15 min, (b) 30 min, (c) 45 min, (d) 60 min, (e) 90 min, and (f) 120 min, at maximum chamber temperature. (g) Plot showing variation in average nanowire core and shell widths as a function of growth time, as determined from TEM analysis. (h) Plot illustrating variation in the core/shell area ratio as a function of growth time.

the growth process. SEM images corresponding to each of these synthesis times are shown in Figure 3. Although ZnS/SiO_2 nanowires were synthesized with growth times as short as 15 min, nanowire alignment was not observed in growth times shorter than 45 min. Longer synthesis times corresponded in general to longer and denser growth product. Although Figure 3f appears to show a lower density of nanowires compared to previous images, this is not the case, as this image is taken at higher magnification to show greater sample detail. Note that the images in Figure 3 are rotated 90° relative to those in Figure 1, such that the flow gas here is indicated to be in the vertical direction.

Several analysis techniques were performed to compare samples of varying synthesis times. First, a TEM-based study of the various widths of the ZnS core and the SiO_2 shell was conducted. This consisted of measuring, via TEM images, the widths of both the core and the shell and comparing them according to synthesis time. With measurement of over 30 nanowires from each of the six time intervals, the average (mean) widths of core and shell for nanowires in each section were determined. While core widths were measured directly, shell widths were determined by subtracting the core size from the total width of the nanowire. A graph of these data is shown in Figure 3g. Not included on this graph are measurements for the 30-min synthesis time interval. These values were omitted as outliers, determined initially by distortion of the graphs, and then confirmed via a standard statistical analysis technique in which the values were found to lay more than one standard deviation away from the next closest data point. For completeness, it should be noted that measurements on samples run in the 30-min interval confirmed the overall trend observed in other samples, showing an average ZnS core size of 13.84 nm and a silica shell width average of 1.59 nm. As can be seen in the graph, the ZnS core tends to become smaller over time (although only by a maximum of a few nanometers) while the SiO_2 shell grows larger with longer synthesis times.

While core and shell width values differ between samples according to time interval, we observed that each nanowire maintains a constant width along its entire length, without the presence of dips or tapering. Therefore the nanowires' relative volumes should be able to be determined from their respective widths according to the following equation:

$$\frac{\text{core volume}}{\text{shell volume}} = \frac{r_c^2}{[(r_c + w_s)^2 - r_c^2]} \quad (1)$$

Here $r_c = w_c/2$ is the radius of the ZnS core and w_s is the thickness of the SiO_2 shell. Results of this analysis for nanowires in each time interval are shown in Figure 3h. As seen in this figure, we found that the core volume relative to the shell volume decreases over time.

While TEM analysis supplied detailed information regarding the nature of a small subset of nanowires in each sample, X-ray diffraction (XRD) techniques were utilized to provide a better understanding of the global nature of the nanowires. In particular, we sought to investigate the overall changes in relative core and shell thickness with respect to synthesis time, for an area of nanowires measuring a few square millimeters. Six samples were examined, each differing only according to

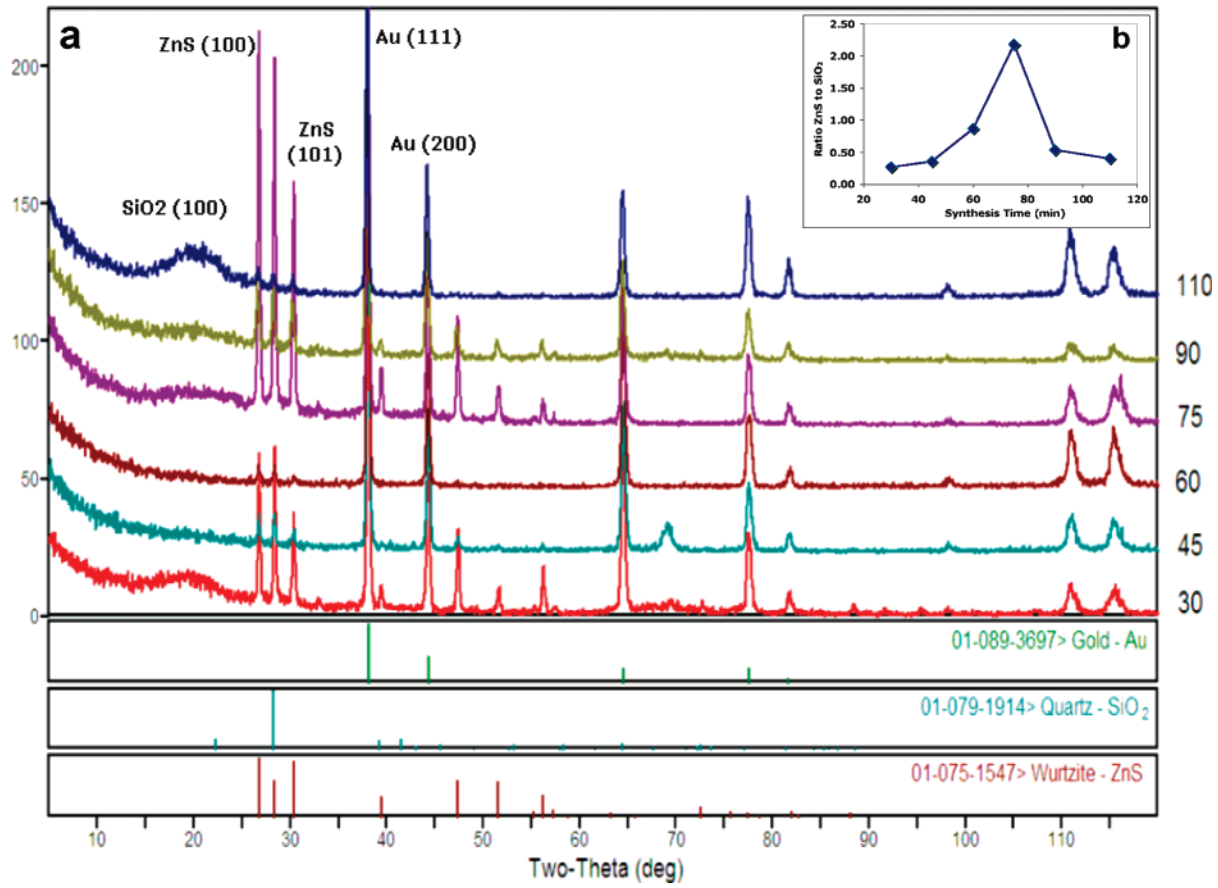

Figure 4. (a) Series of XRD patterns from samples with reaction times varying from 30 to 110 min. (b) Plot illustrating the ZnS:SiO_2 ratio in nanowire samples as a function of reaction time, derived from XRD pattern semiquantitative phase analysis.

experimental reaction time, as in the quantitative TEM analysis. These times were 30, 45, 60, 75, 90, and 110 min. The results of scans from each sample are shown in Figure 4a.

Note that while intensities vary, scans show similar peak profiles for each sample. This result confirms that the experimental design and sample preparation were such that phases remained consistent and no contamination occurred. Variations in intensity may occur for many reasons, including instrumental effects, sample alignment, nanowire density, relative phase concentration, crystallite size, and preferred sample orientation, among others. Phase identification of the diffraction pattern in Figure 4a using PANalytical X-Pert HighScore Plus software yielded three known phases: Au (PDF No. 89-3697); the wurtzite phase of ZnS (PDF No. 75-1547); SiO_2 (PDF No. 82-0512). MDI Jade7.5 software was later used to confirm phase results. To determine relative ZnS and SiO_2 core and shell thickness from the XRD data, we utilized semiquantitative phase analysis for the ZnS phase. HighScore and Jade software were employed to perform the XRD analysis.

The semiquantitative analysis in X'Pert HighScore works on the basis of reference intensity ratio (RIR) values, which divide the intensity of the pure phase to be determined by the intensity of a standard material, often corundum (Al_2O_3). To perform analysis on a sample containing multiple phases, we use the normalized RIR method developed and published by Chung.[29] The normalization used in this method assumes that the sum of all identified phases is 100%. This means that unidentified or amorphous phases will reduce the meaning and accuracy of this analysis. In the case of our samples, TEM found the SiO_2 shell to be mostly amorphous in nature, which was validated through broad peak signatures in the XRD pattern. In such cases, the result is still a good estimate of the relative mass fractions of the identified phases. Since our investigation seeks simply to find the relative differences between ZnS and SiO_2 in the sample rather than actual empirical values for these, we believe this method is reasonable for our purposes. Figure 4b shows a graph illustrating the relative concentration of ZnS versus SiO_2 for each of our samples, as reaction time increases. Note again that, due to the presence of some amorphous SiO_2 in the sample and the possibility of an oxidation layer on the silica substrate surface, these values must be regarded as indicative of a trend rather than as stand-alone empirical values.

Through the use of semiquantitative phase analysis on XRD diffraction patterns produced by samples created at varying reaction times, we have been able to show a clear trend in the variation of core size in the ZnS/SiO_2 core−shell ultralong nanowires as reaction time progressed in our experiments, illustrated in Figure 4b. At short reaction times, both the relative percentage of ZnS in the nanowires and the average size of the ZnS wurtzite crystal begin at a low base value. As the reaction progresses, the ZnS core grows larger, and a larger proportion of ZnS is present in the nanowires, relative to the SiO_2 amorphous shell. As the reaction continues, however, the size of the core appears to reach a maximum value, and then the ZnS again decreases, both in size and concentration.

Last, the photoluminescence spectra are compared for the samples grown at different time periods. The resulting graphs are shown overlaid in Figure 5. All of the spectra show at least two distinct peaks. One peak appears at 340 nm, and the other, around 532 nm. The lower wavelength peak is well-explained as a pure ZnS PL peak. This peak is associated with a material band gap of about 3.65 eV, a good match with the theoretical wurtzite value of 3.91 eV. Because ZnS with very few defects, vacancies, or interstitials is conventionally difficult to find, in

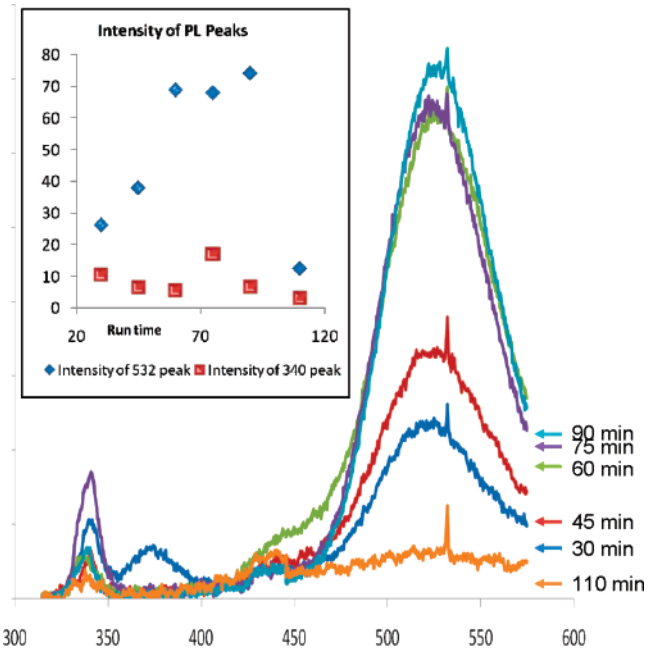

Figure 5. Composite of photoluminescence data from several ultralong ZnS−SiO_2 core−shell nanowire samples. Each pattern corresponds to a unique sample exposed to synthesis conditions for a time interval between 30 and 110 min. The inset illustrates a plot of this data, correlating peak intensities with reaction time.

the literature it is rare to see the 340 nm ZnS peak. However, for nanostructures such as these, which are well-structured and contain few defects compared to bulk materials, the presence of this peak is not surprising. The 532 nm peak is significantly more common. It is associated with Zn defects, vacancies, and interstitials in the ZnS crystal. This peak translates into a band gap of 2.33 eV.[11,30] The sharp peak that appears to be convoluted with the much broader signature around 540 nm is due to an instrumental effect and is present in all profiles originating from the PL equipment used for this analysis.

In the lowest growth time measured, that of 30 min, a broad peak can also be observed at 375 nm, which corresponds to a band gap of 3.30 eV. This peak has been shown to exist in studies of pure silica.[31] This result indicates the possible presence of a silica layer on the substrate surface, exhibiting observable luminescence only in the sample with the lowest density of nanowires. It is important to compare the intensities of the peaks and how they change with longer synthesis times. This is shown more clearly in the inset of Figure 5. Focusing on the 532 nm peak, we observe an interesting phenomenon. The intensity of the peak increases with increasing synthesis times from 30 up to 90 min. However, for nanowires allowed to grow for 110 min, the peak disappears. Also, the ratio between the two major peaks increases with longer synthesis times from 30 to 90 min. Again, at the 110 min measurement, the ratio drops dramatically.

Discussion

Since the first observations of catalyst assisted PVD (physical vapor deposition) nanowire synthesis, researchers have sought to identify underlying growth mechanisms governing the production of these materials. Although much progress has been made, in many cases 1D PVD synthesis remains as a kind of "black box" in which parameters are set, experiments are run, and a final product is achieved without a full understanding of the processes combining to deliver the result. Observation of a metal catalyst particle at the nanowire tip is no longer considered sufficient evidence to support the classic VLS formation process in whole or in part, especially in light of studies with GaAs and InAs structures and other metal catalysts, which seem to indicate that nanowires can be grown by particles remaining in the solid state throughout the synthesis process.[24,32] Studies on Sn-catalyzed ZnO 1D nanostructures indicate that the crystalline and electronic structures of the substrate, nanostructure, and catalyst particle can all play a role in determining the nature of the final growth product.[33,34] In the case of gold-catalyzed ZnS, Si, and SiO_2 1D nanostructures, much has been written regarding possible formation mechanisms specific to synthesized products. In the examination of the wealth of literature on these structures, some general trends can be identified.

Silicon appears most often to form nanostructures via bulk diffusion through the Au catalyst particle. Rarely is silicon observed as a tube or shell structure. A recent publication in which successful synthesis of ZnS−Si core−shell nanowires was achieved reports this result through templating of the silicon onto a previously grown ZnS nanowire and not direct PVD growth.[6] The paper by Wagner on this topic has been previously mentioned, and other papers report in-situ observation of the classic VLS process in Si nanowire systems.[35] The literature also suggests that ZnS nanostructures may form primarily by bulk transport means, as 1D nanostructures of this material also tend toward formation of solid products and core, rather than shell, components. Further evidence has been supplied through EDS analysis, as in the case of one recent study reporting that an EDS detector fit to a TEM revealed traces of Zn and S as well as Au when focused on the terminating Au particle of a ZnS nanowire.[36] Another publication has presented AFM data indicating that Au catalyst islands grew in volume just prior to growth of ZnS nanowires, suggesting that arriving species were diffusing into the catalyst material.[37]

Conversely, SiO_2 commonly appears as a shell or as a tubular structure, frequently forming coating layers over other growth products and in some cases even capping the metal particle.[38] Such behavior is not surprising when considered in light of silica's reduced solubility in gold compared to elemental Si. It is not uncommon to observe areas of increased gold mobility on silicon substrates with localized oxidation, as demonstrated in earlier reports, in which low Si nanowire growth and high Au mobility were correlated to locally oxygen-rich regions on a Si substrate.[38,39] This phenomenon has even been demonstrated as an effective technique for patterning of gold particles on selectively etched Si−SiO_2 wafers.[40] In the case of our experiments, the Si substrates were the only source of silicon in our experiments, while oxygen species likely originated from residues left in the reaction chamber or even from slight oxidation of the substrate surface. Additionally, SiO may have acted as an intermediate in the process.

Still, exactly how these processes occur remains a source of debate. Mass diffusion through the metal particle, surface diffusion around the metal particle, selective incorporation entirely at the particle−nanowire interface, transport up the sides of the growing nanowire, and direct adsorption onto the nanowire have all been identified as possible formation mechanisms in ZnS and SiO_2 1D nanostructures.[41] To help identify the mechanism responsible for the growth of our nanostructures, each of these possible mechanisms was examined with regard to observations of the final ZnS−SiO_2 nanowire growth product. It was determined that any of four distinct growth processes could reasonably be suggested for the growth of our ZnS−SiO_2 nanowire structures. Each of these is examined schematically in Figure 6.

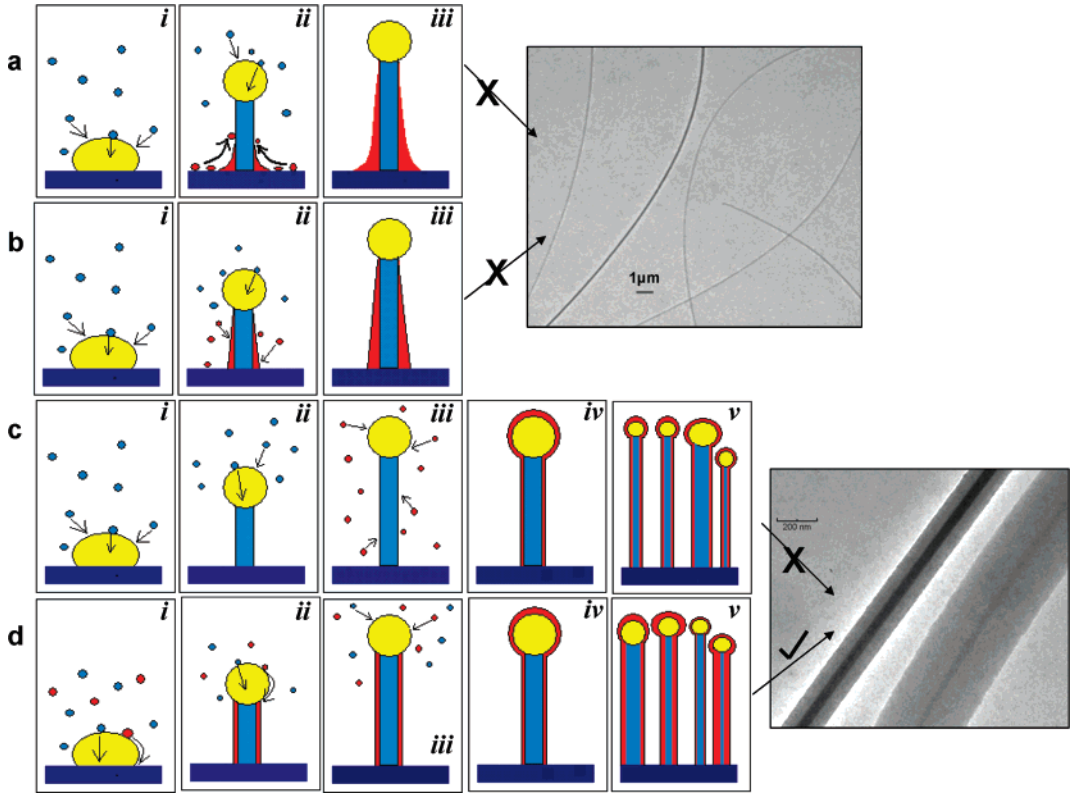

Figure 6. Schematic illustrating possible sample formation mechanisms and corresponding TEM images. Here yellow signifies Au, dark blue represents the Si substrate, light blue represents ZnS, and red coloration is used for SiO_2. (a) In this model, ZnS species are preferentially attracted to the Au catalyst particle and migrate to form the nanowire core. SiO_2 species form and migrate up the sides of the ZnS nanowire. (b) This model is similar to (a) except here silica species adsorb as gaseous species rather than migrating up the ZnS nanowire from its base. Our final TEM image shows that these mechanisms are unlikely, since our samples demonstrate uniform shell thickness along their entire length. (c) In this model, the ZnS nanowire forms first and then is completely encased in an amorphous silica coating. If this were the case, the silica coating should be the same thickness for all nanowires in a sample. The included TEM image demonstrates that this condition is not observed. (d) The proposed formation mechanism: ZnS diffuses through the bulk of the Au catalyst droplet and forms the crystalline nanowire core while SiO_2 species travel around the droplet surface to create the amorphous shell. This is the model suggested by our analysis.

Figure 6a illustrates a growth process in which ZnS molecules diffuse through or around the gold catalyst particle, with silica species originating on the substrate surface and moving up the sides of the growing nanowire. A similar process is illustrated in Figure 6b; however, here the shell is formed via direct adsorption of silica species from the gas phase. For very long nanostructures containing an amorphous silica shell, synthesis via these processes is likely to produce structures that vary in thickness along the length.[21,42] In short, we would expect to find variations in silica shell thickness along a single nanowire. In the first case, this phenomenon would likely occur due to the increasing distance that the silica species would have to travel up the nanowire to reach close to the tip. In the latter case, the portion of the nanowire forming earliest, or that at the bottom, would be exposed to the silica vapor for a longer period and, therefore, should form a thicker shell. An amorphous silica layer like that observed in our samples would likely not experience a strong enough driving force to promote the SiO_2 species up the nanowire such that newly formed ZnS core material at the top would maintain exactly the same shell thickness as earlier areas near the substrate surface. As can be shown in the last image of these figures, nanowires in our samples demonstrate uniform thickness along their entire length, sometimes of several hundred microns, suggesting that neither of these mechanisms is applicable for their formation.

Another possible synthesis route is presented in Figure 6c. The process depicted here can be considered as similar to an atomic layer deposition (ALD) process in two steps, in which the ZnS nanowire forms first and then is uniformly coated with an amorphous silica shell. Previous reports have cited this process as a possible formation mechanism for silica nanotubes in which the metal catalyst particle becomes completely encased.[41] However, as shown in part v of this figure, such a mechanism would yield nanowires with completely uniform shell thickness, despite any variations in core size or structure. Much as in a conventional ALD process, we would expect to observe similar shell thickness among *different* nanowires in a single sample, since at the time of silica deposition the ZnS core would not be exhibiting dynamic growth. The image shown in conjunction with Figure 6c, which illustrates significant variation in shell thickness between nanowires from the same sample, indicates that, for our synthesis, such a result is not observed. Therefore, the most probable nanowire formation mechanism in our samples is that illustrated in Figure 6d. This series of images describes a process in which ZnS diffuses through the Au particle to form the nanowire core and SiO_2 travels on the surface of the Au particle to the nanowire interface in a simultaneous and dynamic growth process. Variations in particle size and surface contact angle, among other factors, likely lead to observed thickness variations in the core and shell portions of our ultralong nanowires.

On the basis of this proposed growth model, the results of the systematic analysis were examined. Our TEM studies indicated that the size of the silica shell increased over time, while the ZnS core remained relatively the same, with a slight decrease in size. XRD analysis likewise suggested an initial increase in the ZnS core material with increase in reaction time; however, this increase peaked near 60−75 min and then

declined. It is interesting that the description offered in the XRD data differs somewhat from the trend revealed through our TEM analysis. Each technique contains inherent sources of error. TEM analysis provides useful information regarding a small subset which may not be typical of a much larger sample. Sources of error in our XRD techniques have been described previously. It is also possible that what appears as a disparity is, in fact, simply differences due to analysis methods. Since the XRD techniques plotted ZnS core *ratio*, if after the peak synthesis time the silica shell thickness increased or the ZnS core incorporated more defects, the XRD signatures could report a ZnS size decrease while the actual ZnS size remained constant.

Photoluminescence data were likewise employed to explore the development of our ultralong nanowires at each time interval. Some studies have shown that SiO_2 passivation layers on Si have the effect of increasing the intensity of measured photoluminescence peaks. In fact, the intensity of the emission has been shown to correlate to the degree of surface passivation on the films. The SiO_2 shell in our samples could have the same effect on the ZnS core's luminescence. This, along with the XRD suggesting that the ZnS core is initially increasing, would explain the increase in intensity of the 532 nm peak. What remains unexplained is the complete disappearance of this peak at very long synthesis run times. Several explanations are plausible. The ZnS core may be so reduced that the intensity of the 532 nm peak greatly diminishes. Because this peak is associated with defects in the crystal structure, it could be that the defects are too energetic to remain in the ZnS core with the annealing time (growth time) being long. This explanation, however, is not supported by our other data. It is also possible that the SiO_2 shell is so large that it eclipses the effective luminescence of the much smaller ZnS core.

On the basis of the trends revealed in our semiquantitative XRD analysis, we can begin to describe the nanowire growth process as it evolved in time. Most of our data suggest that as synthesis time increased, the silica shell thickness also increased. The shell thickness increase is easily explained as a function of increased number of available species in a very fast and efficient surface diffusion growth process. The size variation of the ZnS core is somewhat under debate; however, both the PL and XRD data support an initial increase and then decrease of the ZnS core size *relative* to the silica shell. Because we know the shell thickness increases as time evolves, the indication of a decrease in these analyses could be due simply to the role of a thicker SiO_2 layer, with the ZnS core size remaining the same. Whether the ZnS grew to a maximum size and then decreased or whether the average core size remained mostly unchanged after this period, such a peak in core thickness suggests that at 60−75 min there exists a set of conditions producing ideal growth of these structures, i.e., high-quality aligned nanowires of greatest length and density.

Interestingly, when experimental conditions were kept consistent for producing the ultralong core−shell nanowires but the thickness of the gold catalyst layer was reduced (below 20 nm), the synthesized product changed dramatically, producing short, unaligned, low-density structures. Therefore, we know that the gold catalyst layer must be a key component in the formation of these ultralong nanowires. Several prior publications cite the critical influence of the Au−Si alloy in formation of Si nanowires, and the Au−Si phase diagram shows that such an alloy allows for a dramatically reduced temperature at which the material exhibits a liquid phase. The presence of a thick gold layer coupled with the elevated chamber temperature may have facilitated a formation of a Au−Si eutectic alloy on the substrate surface. In-situ analyses have shown that, in the case of Au on Si, an alloy layer is formed on the substrate surface which then quickly nucleates spherical Au particles. These continue to agglomerate until large enough to sustain nanowire growth. The Gibbs−Thomson effect places a lower limit on the width of wires which can grow under a given set of conditions, such that very small catalyst particles cannot sustain growth due to an effective wire chemical potential greater that that of the vapor phase. Whether through formation of a eutectic or simply gold migration, thinner gold layers most likely cannot sustain high-density production of these small yet growth-sustaining Au catalysts needed for the formation of our fine, dense, and ultralong nanowires.

Such a result explains the role of the thick gold layer but not the observed maximum in ZnS core thickness occurring at intermediate synthesis times. SEM observation of a 20 nm gold-coated substrate imaged prior to and after exposure to the same experimental conditions but without the presence of ZnS powder indicates that while the surface initially appears like a rough film, after just 15 min at elevated temperature before cooling, the gold on the surface migrated to form regions of large islands and small particles. Prior publications have established that similarly to very small gold particles, those above a certain size also do not promote as efficient nanowire growth as those with higher surface contact angles. It is likely that, at short synthesis times, only the smaller more ideal catalyst sites initiated nanowire growth, while longer synthesis times allowed the larger less efficient sites began to nucleate ZnS nanowires. Therefore, we find that the growth of ultralong ZnS−SiO_2 core−shell nanowires depends upon the presence of gold catalyst particles of a size within an ideal range. Above or below a critical size, gold islands do not support nanowire growth, leading to a peak in ZnS core size at around 60−75 min growth time and only with a sufficiently thick substrate surface gold layer. As discussed previously, the ZnS nanowire core forming via bulk diffusion through the gold catalyst is critically dependent on the size and condition of the catalyst particle. The Si species, however, most likely combines with residual oxygen in the chamber before diffusing around the catalyst particle to form an amorphous silica coating and is much less critically dependent on Au particle size.

Finally, theoretical calculations were performed to determine the feasibility of this growth model. We set out to determine if our dual diffusion model could be reasonably predicted according to general diffusion relations. For this analysis we chose to assume the case of bulk diffusion for ZnS and then worked to find the resulting diffusion constant for SiO_2. Absorption operations involve contact of a gas mixture with a liquid and preferential dissolution of a component in the contacting liquid. Depending on the chemical nature of the involved molecules, the absorption may or may not involve chemical reaction. This calculation was based on the expression for adsorption of a gas in a liquid with a chemical reaction at the interface:

$$N_A|_{Z=0} = \frac{D_{AB}C_{A0}}{\delta}\left[\frac{\sqrt{k/D_{AB}}\delta}{\tan h(\sqrt{k/D_{AB}}\delta)}\right] \qquad (2)$$

Here N_A is the flux of species A through the liquid, D_{AB} is the diffusivity of species A in B, C_{AO} is the maximum concentration of arriving species at the liquid surface, and δ is the distance that the diffusing species must travel, here taken to be the diameter of the catalyst droplet. This equation assumes a constant diffusivity and a low concentration of A in the liquid such that the liquid interface contains plenty of adsorption sites.

The constants of this equation can be evaluated from the boundary conditions:

$$Z = 0: \quad C_A = C_{A0}$$

$$Z = \delta: \quad C_A = 0 \tag{3}$$

With careful evaluation of eq 2 it is apparent that the term

$$[\sqrt{k/D_{AB}}\delta/(\tan h(\sqrt{k/D_{AB}}\delta))] \tag{4}$$

describes the influence of the chemical reactions at the liquid interface. This term is a dimensionless quantity, often termed the Hatta number. If the chemical reaction at the interface is neglected (a reasonable assumption due to the unchanged state of the ZnS precursor in the final nanowire chemistry), the simplified expression correlating flux and diffusivity is

$$N_A \approx (D_{AB})(C_{AO})/\delta \tag{5}$$

which is the equation we used for our calculations.

Here, we let the diameter of the catalyst particle, δ, equal 40 nm. To find the concentration of each gaseous species, we assume an ideallike behavior and note that the evaporation temperature of Si (and SiO_2) is approximately twice that of ZnS. In this case the total pressure is taken to be a simple sum of the partial pressure contributed by each species. Since the relative thicknesses of the core and shell in our nanowires did not fluctuate or taper, we constrained the flux of ZnS molecules to be equivalent to that of SiO_2 species at the nanowire−gold interface. The diffusivity of ZnS was found by observing the average experimental nanowire growth rate and applying this to the molecular system. For ZnS, the diffusivity, $D_{AB'}$ was found to be $\sim 8 \times 10^{-6}$ cm^2/s. This value is well within the range of bulk diffusion through a liquid. Equation 5 was then used to find the flux for ZnS. This value was then fixed for the case of SiO_2, and the diffusivity was calculated. This value was found to be 0.16 cm^2/s, a very high diffusivity, best explained by a surface diffusion mechanism. Therefore, our calculations attest to the theoretical feasibility of our proposed growth model, in which the ZnS core was formed by volume diffusion across the catalyst particle while the silica shell was formed by surface diffusion on the catalyst particle.

Conclusion

Core−shell $ZnS-SiO_2$ nanowires with widths on the order 30 nm and up to 1 cm in length were synthesized through a simple vapor deposition process. The nanowires were aligned as-synthesized along the direction of the gas flow in the system. All nanowires in grown samples were shown to contain a crystalline ZnS core surrounded by an amorphous SiO_2 shell. Their growth was analyzed experimentally, comparing varying synthesis time and subsequent product using SEM, TEM, XRD, and PL techniques. We investigate the growth mechanism of these core−shell nanowires, utilizing literature, calculation, and detailed characterization to arrive at a proposed novel VLS growth mechanism in which both volume and surface diffusion occur simultaneously for different chemical species in the gold catalyst particle. This is the first known report of such long aligned core−shell nanowires and the first known proposal of a simultaneous dual-diffusion mechanism of different chemical species for the VLS growth of nanowires.

Acknowledgment. This work was supported by Emory-Georgia Tech CCNE funded by the NIH. D.M. and J.R.M. contributed equally to this work.

References and Notes

(1) Moore, D. F.; Ding, Y.; Wang, Z. L. *J. Am. Chem. Soc.* **2004**, *126*, 14372.
(2) King, C. N. *J. Vac. Sci. Technol., A* **1996**, *14*, 1729.
(3) Rosenberg, R. A.; Shenoy, G. K.; Heigl, F.; Lee, S. T.; Kim, P. S. G.; Zhou, X. T.; Sham, T. K. *Appl. Phys. Lett.* **2005**, *86*.
(4) Xu, X. J.; Fei, G. T.; Yu, W. H.; Wang, X. W.; Chen, L.; Zhang, L. D. *Nanotechnology* **2006**, *17*, 426.
(5) Erwin, S. C.; Zu, L. J.; Haftel, M. I.; Efros, A. L.; Kennedy, T. A.; Norris, D. J. *Nature* **2005**, *436*, 91.
(6) Hu, J. Q.; Bando, Y.; Liu, Z. W.; Zhan, J. H.; Golberg, D.; Sekiguchi, T. *Angew. Chem., Int. Ed.* **2004**, *43*, 63.
(7) Xia, Y. N.; Yang, P. D.; Sun, Y. G.; Wu, Y. Y.; Mayers, B.; Gates, B.; Yin, Y. D.; Kim, F.; Yan, Y. Q. *Adv. Mater.* **2003**, *15*, 353.
(8) Fang, X. S.; Ye, C. H.; Zhang, L. D.; Wang, Y. H.; Wu, Y. C. *Adv. Funct. Mater.* **2005**, *15*, 63.
(9) Fang, X. S.; Zhang, L. D. *J. Mater. Sci. Technol.* **2006**, *22*, 721.
(10) Lin, M.; Sudhiranjan, T.; Boothroyd, C.; Loh, K. P. *Chem. Phys. Lett.* **2004**, *400*, 175.
(11) Fan, X.; Meng, X. M.; Zhang, X. H.; Wu, S. K.; Lee, S. T. *Appl. Phys. Lett.* **2005**, *86*.
(12) Lieber, C. M. *Solid State Commun.* **1998**, *107*, 607.
(13) Morales, A. M.; Lieber, C. M. *Science* **1998**, *279*, 208.
(14) Ravindran, S.; Chaudhary, S.; Colburn, B.; Ozkan, M.; Ozkan, C. S. *Nano Lett.* **2003**, *3*, 447.
(15) Michalet, X.; Pinaud, F. F.; Bentolila, L. A.; Tsay, J. M.; Doose, S.; Li, J. J.; Sundaresan, G.; Wu, A. M.; Gambhir, S. S.; Weiss, S. *Science* **2005**, *307*, 538.
(16) Mattoussi, H.; Mauro, J. M.; Goldman, E. R.; Anderson, G. P.; Sundar, V. C.; Mikulec, F. V.; Bawendi, M. G. *J. Am. Chem. Soc.* **2000**, *122*, 12142.
(17) Akerman, M. E.; Chan, W. C. W.; Laakkonen, P.; Bhatia, S. N.; Ruoslahti, E. *Proc. Natl. Acad. Sci. U.S.A.* **2002**, *99*, 12617.
(18) Patolsky, F.; Zheng, G. F.; Lieber, C. M. *Anal. Chem.* **2006**, *78*, 4260.
(19) He, J. H.; Zhang, Y. Y.; Liu, J.; Moore, D.; Bao, G.; Wang, Z. L. *J. Phys. Chem. C* **2007**, *111*, 12152.
(20) Wagner, R. S.; Ellis, W. C. *Appl. Phys. Lett.* **1964**, *4*, 89.
(21) Givargizov, E. I. *J. Cryst. Growth* **1975**, *31*, 20.
(22) Yiying, Wu, P. Y. *J. Am. Chem. Soc.* **2000**, *123*, 3165.
(23) Dailey, J. W.; Taraci, J.; Clement, T.; Smith, D. J.; Drucker, J.; Picraux, S. T. *J. Appl. Phys.* **2004**, *96*, 7556.
(24) Persson, A. I.; Larsson, M. W.; Stenstrom, S.; Ohlsson, B. J.; Samuelson, L.; Wallenberg, L. R. *Nat. Mater.* **2004**, *3*, 677.
(25) Wang, Y. W.; Zhang, L. D.; Liang, C. H.; Wang, G. Z.; Peng, X. S. *Chem. Phys. Lett.* **2002**, *357*, 314.
(26) Li, Y. J.; You, L. P.; Duan, R.; Shi, P. B.; Du, H. L.; Qiao, Y. P.; Qin, G. G. *Nanotechnology* **2004**, *15*, 581.
(27) Wang, Z. W.; Daemen, L. L.; Zhao, Y. S.; Zha, C. S.; Downs, R. T.; Wang, X. D.; Wang, Z. L.; Hemley, R. J. *Nat. Mater.* **2005**, *4*, 922.
(28) Freitas, R. A. Private communucation, 2003.
(29) Chung, F. H. *J. Appl. Crystallogr.* **1974**, *7*, 519.
(30) Murugan, A. V.; Heng, O. Y.; Ravi, V.; Viswanath, A. K.; Saaminathan, V. *J. Mater. Sci.* **2006**, *41*, 1459.
(31) Leone, M.; Agnello, S.; Boscaino, R.; Cannas, M.; Gelardi, F. M. *Phys. Rev. B* **1999**, *60*, 11475.
(32) Dick, K. A.; Deppert, K.; Martensson, T.; Mandl, B.; Samuelson, L.; Seifert, W. *Nano Lett.* **2005**, *5*, 761.
(33) Gao, P. X.; Ding, Y.; Wang, I. L. *Nano Lett.* **2003**, *3*, 1315.
(34) Gao, P. X.; Wang, Z. L. *J. Phys. Chem. B* **2004**, *108*, 7534.
(35) Kodambaka, S.; Tersoff, J.; Reuter, M. C.; Ross, F. M. *Phys. Rev. Lett.* **2006**, *96*.
(36) Holmes, J. D.; Johnston, K. P.; Doty, R. C.; Korgel, B. A. *Science* **2000**, *287*, 1471.
(37) Westwater, J.; Gosain, D. P.; Usui, S. *Phys. Status Solidi A* **1998**, *165*, 37.
(38) Song, J. H.; Wang, X. D.; Riedo, E.; Wang, Z. L. *J. Phys. Chem. B* **2005**, *109*, 9869.
(39) Kwon, S. J.; Park, J. G. *J. Phys.: Condens. Matter* **2006**, *18*, 3875.
(40) Cussler, E. L. *Diffusion: mass transfer in fluid systems*, 2nd ed.; Cambridge University Press: New York, 1997.
(41) Wang, H. Y.; Fischman, G. S. *J. Appl. Phys.* **1994**, *76*, 1557.
(42) Wang, Y. W.; Schmidt, V.; Senz, S.; Gosele, U. *Nat. Nanotechnol.* **2006**, *1*, 186.